Channel Estimation for Multiple-Input Multiple-Output Orthogonal Chirp-Division Multiplexing Systems

Xing Ouyang, *Member, IEEE*, Octavia A. Dobre, *Fellow, IEEE*, Yong Liang Guan, *Senior Member, IEEE*, and Paul Townsend, *Senior Member, IEEE*

***Abstract*— In multiple-input multiple-output (MIMO) systems, channel estimation is of crucial importance to guarantee reliable recovery of ultra-high-speed MIMO signals. This paper proposes a novel channel estimation algorithm for the emerging MIMO-based orthogonal chirp-division multiplexing (OCDM) systems by utilizing the unique features of OCDM signals. In the proposed algorithm, a set of pilot signals is designed based on the Fresnel basis, which is essentially a family of orthogonal linear chirps. The pilots are assigned to different antennas for transmission occupying the same time slot and bandwidth. According to the convolution-preservation theorem of the Fresnel transforms, the transfer matrices of MIMO-OCDM systems can be readily estimated at the receiver without any inter-antenna interference, even if the pilots overlap in both the time and frequency domains. The proposed algorithm avoids bandwidth waste in conventional channel estimators, in which silent pilots will be required in time and/or frequency to ensure the received MIMO pilots separable. We show that the proposed algorithm is unbiased for the unique OCDM pilots and has better estimate accuracy and system performance. Finally, analysis and numerical results are provided to validate its advantages as a promising algorithm for emerging wireless access technology based on MIMO-OCDM.**

***Index Terms*— Channel estimation, orthogonal chirp-division multiplexing (OCDM), multiple-input multiple-output (MIMO), orthogonal frequency-division multiplexing (OFDM), chirp spread spectrum (CSS), Fresnel transform, pulse compression.**

Manuscript received 14 July 2022; revised 14 January 2023 and 24 April 2023; accepted 14 May 2023. Date of publication 25 May 2023; date of current version 9 January 2024. This work was supported in part by the Irish Research Council (IRC) under Grant GOIPD/2021/875 and Grant IRCLA/2022/3636, in part by the Science Foundation Ireland (SFI) under Grant SFI-12/RC/2276_P2_IPIC, and in part by the Enterprise Ireland (EI) under Grant CF-2021-1678-P. The work of Octavia A. Dobre was supported in part by the Natural Sciences and Engineering Research Council of Canada (NSERC) through its Discovery Program. An earlier version of this paper was presented in part at the 2022 IEEE GlobeCom Workshop WS08 [DOI: 10.1109/GCWkshps56602.2022.10008784]. The associate editor coordinating the review of this article and approving it for publication was R. Dinis. *(Corresponding author: Xing Ouyang.)*

Xing Ouyang and Paul Townsend are with the Photonic Center, Tyndall National Institute, University College Cork, Cork, T12 R5CP, Ireland (e-mail: xing.ouyang@tyndall.ie; paul.townsend@tyndall.ie).

Octavia A. Dobre is with the Faculty of Engineering and Applied Science, Memorial University of Newfoundland, St. John's, NL A1B 3X7, Canada (e-mail: odobre@mun.ca).

Yong Liang Guan is with the School of Electrical and Electronics Engineering, Nanyang Technological University, Singapore 639798 (e-mail: eylguan@ntu.edu.sg).

Color versions of one or more figures in this article are available at https://doi.org/10.1109/TWC.2023.3278173.

Digital Object Identifier 10.1109/TWC.2023.3278173

I. Introduction

IN RESPONSE to the societal and economic needs for the sixth generation (6G) wireless networks that are expected in the 2030s, research and innovation initiatives are being proactively kicked off globally. Pursuing the vision promised by 6G for enhanced capacity, resilience, and flexibility, the combination of advanced modulation technology with multiple-input multiple-output (MIMO) antenna technology is the key enabler for radio access by fully utilizing the space-time-frequency dimensions of a wireless system. For example, in 4G and recent 5G mobile networks, MIMO orthogonal frequency-division multiplexing (OFDM) has been proven to be a successful air interface solution for enabling high-speed wireless broadband services [1], [2], [3]. However, as signal bandwidth increases into the gigahertz range and carrier frequencies approach the terahertz region, novel waveform modulation technologies will be needed for the 6G air interface, and hence this is becoming a subject of intense study by industry and academia worldwide [4], [5], [6].

Recently, orthogonal chirp-division multiplexing (OCDM) has been proposed as a new advanced modulation technology that is promising for ultra-high-speed communications. OCDM has been theoretically and experimentally demonstrated firstly by the authors in wireless and fiber-optic systems [7], [8], [9], [10] and extended to other applications, such as underwater acoustic communications, integrated radar and communication systems, optical wireless and millimeter-wave systems [11], [12], [13]. These studies have shown that under the same conditions OCDM signals exhibit superior performance compared to OFDM signals. In contrast to OFDM, which divides a high-speed data stream to a large number of narrowband subcarriers parallelly modulated in frequency [14], [15], [16], OCDM synthesizes a large number of linearly frequency-modulated (LFM) (or chirped) waveforms for high-speed data modulation. Essentially, OCDM is a specialized chirp spread spectrum (CSS) technology that achieves the Nyquist signaling rate with optimal spectral efficiency, analogous to OFDM and frequency-division multiplexing (FDM). However, compared to traditional CSS systems, which are notorious for their poor spectral efficiency due to the non-orthogonal chirped waveforms [17], [18], [19], the chirps in OCDM are mutually orthogonal, and thus attain the maximum spectral efficiency at the so-called Nyquist signaling rate [7].

Moreover, by virtue of the spread-spectrum feature inherited from CSS, OCDM shows superior resilience in combating a variety of detrimental effects in communication systems, and thus outperforms other waveform modulation techniques, e.g., OFDM. Thus, one can expect that the combination of MIMO and OCDM technologies can offer a more appealing air interface solution for future broadband systems, such as the beyond 5G and 6G mobile networks, and wireless local area networks (WLAN), offering higher data rate and better reliability.

In MIMO-based systems, accurate channel acquisition is of crucial importance to guarantee reliable recovery of the high-speed MIMO signals [20], [21], [22]. Here, we will focus on pilot-based channel estimation schemes for MIMO-OCDM systems. Although blind channel estimation schemes do not need pilot signals, they have much longer convergence time and are very susceptible to various impairments, especially in the context of MIMO scenarios [23]. We aim to design a channel estimation algorithm dedicated to the MIMO-OCDM systems by fully utilizing the unique features of OCDM signals for enhanced performance and signal compatibility. Although we have studied chirped pilot signals for fiber-optic systems in [24], which is essentially single-input single-output (SISO) systems, there is no dedicated channel estimation algorithm for the case of the MIMO-OCDM systems studied here.

Thanks to the compatibility of OCDM and OFDM signals, the channel estimation algorithms devised for MIMO-OFDM, such as [25], [26], [27], [28], [29], [30], [31], and [32], can be adapted for MIMO-OCDM systems. However, there are some drawbacks in the traditional channel estimation algorithms for the MIMO-based systems which, if not addressed, will also be imposed upon the MIMO-OCDM systems. For example, the spatial dimension of pilot matrices should be no less than the number of transmitting antennas to reconstruct the transfer matrices of a MIMO system. In terms of pilot design, silent symbols are usually required in the time and/or frequency domains to avoid interference between the transmitting antennas [33], [34], [35], [36]. That is, if one antenna is active transmitting a pilot, other antennas should stay silent in the corresponding time and/or frequency domain without emitting any signal. In this way, the transfer matrices can be recovered easily albeit at the cost of a waste of bandwidth by a factor equal to the number of transmitting antennas [37]. Nevertheless, due to their simplicity, channel estimation schemes based on silent pilots have been widely employed in many practical systems, such as 4G and 5G systems [38].

To mitigate the bandwidth loss due to silent pilots, different pilot allocation schemes, such as block, comb, and scatter-type schemes were devised for training [27], [39], [40], [41], [42], [43], [44]. Considering the characteristics of MIMO channels, least square (LS) [45] or linear minimum mean square error (LMMSE) [46] estimators, depending on whether statistical knowledge of the channel is available or not, were proposed to extract channel frequency response (CFR) matrices of MIMO channels. To reduce the pilot overhead, estimators based on time domain or singular valued decomposition (SVD) algorithms were proposed [47], [48], [49], [50]. Although these estimators optimize the pilot overhead with respect to the mean square error (MSE) performance in the corresponding domain, they require complicated matrix operations and need to transform the estimate back to the frequency domain along with interpolation to reconstruct the MIMO transfer matrices, which introduces deviation in the frequency domain. These estimation algorithms devised for MIMO-OFDM systems have been summarized in [20], [31], and [51] and the references therein.

In this paper, we address the question of whether it is possible to design a channel estimation algorithm optimized for the MIMO-OCDM systems. We exploit the unique features of OCDM to propose a novel channel estimation algorithm for MIMO-OCDM systems that is optimized in terms of performance and compatibility with existing OFDM systems. In particular, the novelty and contributions of this work can be summarized as follows.

- A channel estimation algorithm is proposed, which allows the chirped pilots that overlap in both time and frequency domains to be transmitted from all transmitting antennas simultaneously. By utilizing the pulse-compression property of the OCDM signals and the convolution-preservation property of the Fresnel transform, there is no inter-antenna interference for improved accuracy and no silent pilots are needed to avoid spectral efficiency reduction.
- The theoretical MMSE performance of the proposed algorithm is derived to formulate the optimum noise rejection condition considering generic channel delay spreads, which provides guidance for practical implementations. In addition, numerical simulations are carried out to compare the performance with that of other algorithms and to show the advantages of the proposed algorithm.
- The channel estimation algorithm is generalized for an arbitrary number of MIMO antennas, and even for other types of MIMO-based systems, such as MIMO-OCDM/OFDM systems, and massive MIMO systems.
- Considering the compatibility of OCDM and OFDM signals, the proposed algorithm offers an attractive channel estimation solution for a smooth transition between MIMO-OFDM and MIMO-OCDM systems for future wireless system upgrade.

The rest of this paper is organized as follows. In Section II. the system model of the MIMO-OCDM system is formulated. The proposed channel estimation algorithm is introduced in Section III, and the performance of the algorithm is analyzed in comparison with the least-square (LS) algorithm in Section IV. Section V provides the simulation results to study the performance of the proposed algorithm and validate its advantage. Finally, Section VI concludes the paper.

Notation: In this paper, we use italic letters for variables, and boldface lowercase/uppercase letters for vectors/matrices. The superscript, $(\cdot)^*$, is the complex conjugate operator, and $(\cdot)^T$, $(\cdot)^H$, and $(\cdot)^\dagger$ denote the transpose, Hermitian transpose, and pseudo-inverse of a matrix, respectively. Tr$\cdot$ and $\|\cdot\|_F^2$ are the trace and Frobenius norm of a matrix, respectively. $\circledast$ is the circular convolution operator. $\mathcal{E}\{\cdot\}$ denotes the expectation or ensemble average. $\mathcal{F}_\Omega\{\cdot\}$ is the discrete Fourier transform (DFT) and $\mathcal{F}_\Psi\{\cdot\}$ is the discrete Fresnel transform (DFnT).

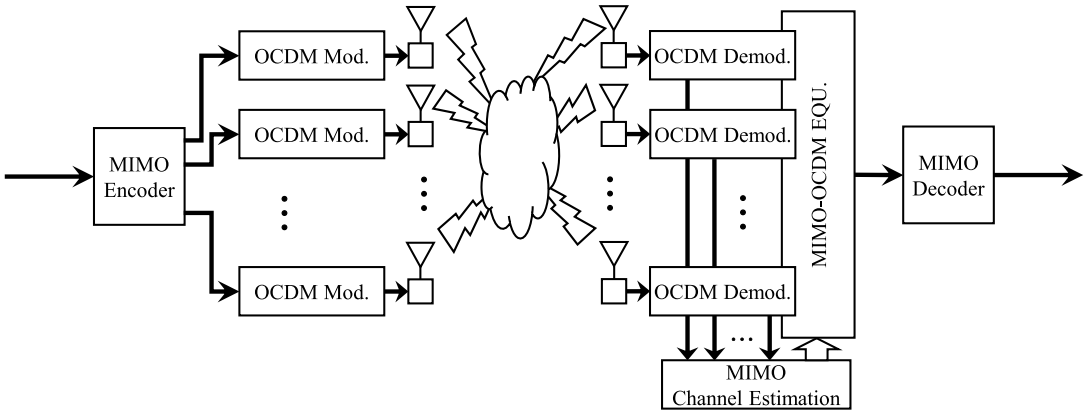

Fig. 1. Block diagram of the proposed MIMO-OCDM system.

II. System Model of MIMO-OCDM

We consider a spatial multiplexing (SM) MIMO system with M_{T} transmitting (TX) and M_{R} receiving (RX) antennas, given that $M_{\mathrm{R}} \geq M_{\mathrm{T}} \geq 1$, as illustrated in Fig. 1. Nevertheless, the proposed channel estimation algorithm and system model can be readily adapted for other types of MIMO systems, such as the space-time block code (STBC) MIMO, for which $M_{\mathrm{R}} < M_{\mathrm{T}}$ is also valid.

At the transmitter, the bit stream is serial-to-parallel (S/P) converted and grouped in blocks and mapped to symbols for modulation. The symbols are then processed by the MIMO encoder and divided into M_{T} streams for waveform modulation. In comparison to OFDM that generates the time-domain signals by DFT, OCDM generates the signal by DFnT [52], which can be efficiently realized using fast Fresnel transform (FFnT) algorithms with the same arithmetic complexity as the fast Fourier transform (FFT). Given that each OCDM symbol consists of N chirps, the discrete-time signal on the q-th TX antenna, $s_q(n)$ for $q = 1, \ldots, M_{\mathrm{T}}$, and $n = 0, 1, \ldots, N-1$, is generated by an inverse DFnT (IDFnT), as

$$\begin{aligned} s_q(n) &= \sqrt{\frac{E_s}{M_{\mathrm{T}}}} \cdot \mathcal{F}_{\Psi}^{-1}\left\{x_q(k)\right\}(n) \\ &= \sqrt{\frac{E_s}{M_{\mathrm{T}}}} \cdot \frac{1}{\sqrt{N}} e^{j\frac{\pi}{4}} \sum_{k=0}^{N-1} x_q(k) \\ &\quad \times \begin{cases} e^{-j\frac{\pi}{N}(k-n)^2}, & N \equiv 0 \pmod 2 \\ e^{-j\frac{\pi}{N}\left(k-n+\frac{1}{2}\right)^2}, & N \equiv 1 \pmod 2, \end{cases} \end{aligned} \tag{1}$$

where $\mathcal{F}_{\Psi}\{\cdot\}$ is the DFnT operator and $\mathcal{F}_{\Psi}^{-1}\{\cdot\}$ is the IDFnT operator, and $x_q(k)$ is the symbol modulating the k-th chirp on the q-th TX antenna, for $k = 0, \ldots, N-1$. Guard intervals (GIs) are inserted between OCDM symbols to confine inter-symbol interference (ISI) from adjacent symbols caused by the delay spread of multipath propagation. Based on the property of DFnT, the GI should be in the form of cyclic prefix (CP) to maintain the circular-convolution. In practice, the length of CP should be sufficiently larger than the maximum delay spread of the channel. The baseband signals are then parallel-to-serial (P/S) converted and up-converted for transmission.

The transmitted signals will propagate through the wireless MIMO channel with attenuation, reflection, and scattering, and arrive at the receiver. We assume that the MIMO channel is quasi-static, i.e., the state of channel remains unchanged within one frame, and varies from frame to frame. At the output of the MIMO system, the received signals are down-converted back to baseband and sampled to digital domain by analog-to-digital converters (ADCs). After synchronization, the OCDM signals are S/P converted with the GIs removed, and grouped into blocks. The received signal on the p-th RX antenna, for $p = 1, \ldots, M_{\mathrm{R}}$, is the superposition of the transmitted signals,

$$r_p(n) = \sum_{q=1}^{M_{\mathrm{T}}} h_{p,q}(n) \circledast s_q(n) + v_p(n), \tag{2}$$

where $h_{p,q}(n)$ is the channel impulse response (CIR) function of the path from the q-th TX antenna to the p-th RX antenna, $v_p(n)$ is the additive noise on the p-th RX antenna, and $\circledast$ is the circular convolution operator. It should be noted in (2) that the circular convolution results from the effect of CP, which converts linear convolution to circular convolution.

Based on [7], single-tap frequency-domain equalization (FDE) can be adapted to efficiently recover the MIMO-OCDM signals. The received signal on the p-th RX antenna is transformed by a DFT to the frequency domain, as

$$\begin{aligned} y_{\Omega(p)}(m) &= \mathcal{F}_{\Omega}\left\{r_p(n)\right\}(m) \\ &= \sum_{q=1}^{M_{\mathrm{T}}} H_{p,q}(m) \cdot \mathcal{F}_{\Omega}\left\{s_q(n)\right\}(m) + w_{\Omega(p)}(m) \\ &= \sqrt{\frac{E_s}{M_{\mathrm{T}}}} \Gamma^*(m) \sum_{q=1}^{M_{\mathrm{T}}} H_{p,q}(m) \cdot \mathcal{F}_{\Omega}\left\{x_q(k)\right\}(m) \\ &\quad + w_{\Omega(p)}(m), \end{aligned} \tag{3}$$

where

$$H_{p,q}(m) := \mathcal{F}_{\Omega}\left\{h_{p,q}(n)\right\}(m)$$

is the channel frequency response (CFR) function from the q-th TX antenna to the p-th RX antenna, $w_{\Omega(p)}(n)$ is the frequency-domain additive noise on the p-th RX antenna, and $\Gamma(m)$ is a phase coefficient, which is in fact the eigenvalue of DFnT with respect to (w.r.t.) DFT. The third equation in (3)

is arrived by using the eigen-decomposition identity of the DFnT, i.e.,

$$\mathcal{F}_{\Omega}\left\{\mathcal{F}_{\Psi}^{-1}\left\{x\left(k\right)\right\}\right\}\left(m\right)=\Gamma^{*}(m)\times\mathcal{F}_{\Omega}\left\{x\left(k\right)\right\}\left(m\right), \quad (4)$$

where $\Gamma^{*}\left(m\right)$ is the m-th eigenvalue of IDFnT w.r.t. DFT.

To facilitate the representation, we formulate the system in matrix form. Stacking the received signal in (3) w.r.t. p, the received signal vector in the m-th frequency bin is

$$\mathbf{y}_{\Omega}\left(m\right)=\sqrt{\frac{E_s}{M_{\mathrm{T}}}}\Gamma^{*}\left(m\right)\mathbf{\Lambda}(m)\cdot\mathbf{x}_{\Omega}\left(m\right)+\mathbf{w}_{\Omega}\left(m\right), \quad (5)$$

where $\mathbf{y}_{\Omega}\left(m\right)=\left[y_{\Omega(1)}(m),\ldots,y_{\Omega(M_{\mathrm{R}})}(m)\right]^{T}$ is the received frequency-domain signal vector, and $\mathbf{x}_{\Omega}\left(m\right)\in\mathbb{C}^{M_{\mathrm{T}}\times1}$ is the DFT of the transmitted symbol vector in the m-th frequency bin with its q-th element defined as

$$x_{\Omega(q)}\left(m\right):=\mathcal{F}_{\Omega}\left\{x_{q}(n)\right\}\left(m\right), \quad (6)$$

where $\mathbf{\Lambda}\left(m\right)\in\mathbb{C}^{M_{\mathrm{R}}\times M_{\mathrm{T}}}$ is the channel transfer matrix,

$$\mathbf{\Lambda}\left(m\right)=\begin{bmatrix}H_{1,1}\left(m\right) & H_{1,2}\left(m\right) & \cdots & H_{1,M_{\mathrm{T}}}\left(m\right)\\ H_{2,1}\left(m\right) & H_{2,2}\left(m\right) & \cdots & H_{2,M_{\mathrm{T}}}\left(m\right)\\ \vdots & \vdots & \ddots & \vdots\\ H_{M_{\mathrm{R}},1}\left(m\right) & H_{M_{\mathrm{R}},2}\left(m\right) & \cdots & H_{M_{\mathrm{R}},M_{\mathrm{T}}}\left(m\right)\end{bmatrix}, \quad (7)$$

and $\mathbf{w}_{\Omega}\left(m\right)\in\mathbb{C}^{M_{\mathrm{R}}\times1}$ is the frequency-domain noise vector.

Based on (5), once the CFR matrix, $\mathbf{\Lambda}\left(m\right)$, is estimated by some channel estimation method, the channel imposed on the received signal can be compensated. The phase $\Gamma^{*}\left(m\right)$ can be easily rotated back as it is a known scalar. For example, if a linear equalizer is adopted, the equalized signal is

$$\hat{\mathbf{y}}_{\Omega}\left(m\right)=\Gamma(m)\mathbf{\Xi}\left(m\right)\cdot\mathbf{y}_{\Omega}\left(m\right), \quad (8)$$

where $\mathbf{\Xi}\left(m\right)$ is the $M_{\mathrm{T}}\times M_{\mathrm{R}}$ equalization matrix on the m-th frequency bin. If the zero-forcing (ZF) criterion is adopted,

$$\begin{aligned}\mathbf{\Xi}_{\mathrm{ZF}}\left(m\right)&=\sqrt{\frac{M_{\mathrm{T}}}{E_s}}\mathbf{\Lambda}^{\dagger}\left(m\right)\\&=\sqrt{\frac{M_{\mathrm{T}}}{E_s}}\left(\mathbf{\Lambda}^{H}\left(m\right)\mathbf{\Lambda}\left(m\right)\right)^{-1}\mathbf{\Lambda}^{H}\left(m\right),\end{aligned} \quad (9)$$

and if the minimum mean square error (MMSE) criterion is adopted,

$$\begin{aligned}&\mathbf{\Xi}_{\mathrm{MMSE}}\left(m\right)\\&=\sqrt{\frac{M_{\mathrm{T}}}{E_s}}\left(\mathbf{\Lambda}^{H}\left(m\right)\mathbf{\Lambda}\left(m\right)+\frac{M_{\mathrm{T}}}{\rho}\mathbf{I}\right)^{-1}\mathbf{\Lambda}^{H}\left(m\right),\end{aligned} \quad (10)$$

where

$$\rho=\frac{E_s}{N_0}$$

is the signal-to-noise ratio (SNR).

After channel equalization, the transmitted symbols on each layer can be readily recovered with another IDFT. Taking the ZF equalizer for example, the symbols on the q-th TX antenna for decision are

$$\begin{aligned}\hat{x}_{q}\left(m\right)&=\mathcal{F}_{\Omega}^{-1}\left\{\hat{y}_{\Omega(q)}\left(m\right)\right\}\left(k\right)\\&=\mathcal{F}_{\Omega}^{-1}\left\{x_{\Omega(q)}\left(m\right)+\hat{w}_{\Omega(q)}\left(m\right)\right\}\left(k\right)\\&=x_{q}\left(k\right)+\hat{w}_{q}\left(k\right),\end{aligned} \quad (11)$$

where $\hat{w}_{\Omega(q)}\left(m\right)$ is the q-th entry of the equalized noise vector in the frequency domain. It should be noted that although ZF equalizer can completely compensate channel, the noise in the vicinity of frequency nulls will be severely enhanced. MMSE equalization can effectively alleviate the noise enhancement problem as the MMSE coefficients approach the matched filter in low SNR regime and the ZF equalizer for high SNR.

III. Proposed Channel Estimation Algorithm Based on Orthogonal Chirped Pilots

In this section, we propose a novel channel estimation algorithm for MIMO-OCDM systems considering signal compatibility, performance, and complexity. Compared to the OFDM-based pilot schemes that allocate the frequency-domain training symbols to subcarriers with complicated matrix operations to extract the transfer matrices of a MIMO channel, the proposed algorithm adopts the OCDM signals as training symbols with simplified operations to estimate the MIMO transfer matrices directly [53].

To introduce the proposed channel estimation algorithm, we define a family of orthogonal chirps based on OCDM signals, $\mathcal{A}_{\Psi}=\{\vec{\psi}_{k}\mid k=0,1,\cdots,N-1\}$, where $\vec{\psi}_{k}$ are in essence the column vectors of an $N\times N$ IDFnT matrix [52]. The n-th element of $\vec{\psi}_{k}$ is defined as

$$\psi_{0}(n)=e^{j\frac{\pi}{4}}\times\begin{cases}e^{-j\frac{\pi}{N}n^{2}}, & N\equiv0 \pmod 2\\ e^{-j\frac{\pi}{N}\left(n-\frac{1}{2}\right)^{2}}, & N\equiv1 \pmod 2\end{cases} \quad (12)$$

for $k=0$, and the rest are the cyclic shift of $\vec{\psi}_{0}$, as

$$\psi_{k}(n)=\psi_{0}(n-k). \quad (13)$$

Utilizing the pulse-compression property of OCDM signals, if we carefully choose a subset of $\mathcal{A}_{\Psi}$ of size-M_{T} as the pilot signals for channel estimation, the pilots can be simultaneously transmitted over the M_{T} TX antennas within a single OCDM symbol period without causing inter-antenna interference. The basic principle is to select a subset of chirped pilots from $\mathcal{A}_{\Psi}$ that are separable after pulse compression, that is, the DFnT operation at the receiver. In other words, if two chirped pilots from any two TX antennas have a spacing larger than the maximum delay spread of the channel, they are distinguishable after pulse compression without any interference. In this way, the receiver is able to recover the CSI of the MIMO system from the received pilot signals by utilizing the pulse-compression property of $\vec{\psi}_{k}$. In the following, we present the main steps of the proposed algorithm.

Suppose that the pilot signal assigned to the q-th TX antenna is $\vec{\psi}_{D_q}$, where $0\leq D_q\leq N-1$ is the index of the chirp on the q-th TX antenna, the transmitted pilot signals are

$$s_{q}\left(n\right)=\sqrt{\frac{E_s}{M_{\mathrm{T}}}}\cdot\psi_{D_q}\left(n\right). \quad (14)$$

Substituting (14) into (2) yields the received pilot signals, and performing DFnT on the received pilot signal on the p-th RX antenna, we have

$$\begin{aligned} y_{\Psi(p)}(m) &= \mathcal{F}_{\Psi}\left\{r_p(n)\right\}(m) \\ &= \sum_{q=1}^{M_{\mathrm{T}}} h_{p,q}(m) \circledast \mathcal{F}_{\Psi}\left\{s_q(n)\right\}(m) + w_{\Psi(p)}(m) \\ &= \sqrt{N\frac{E_s}{M_{\mathrm{T}}}} \sum_{q=1}^{M_{\mathrm{T}}} h_{p,q}(m - D_q) + w_{\Psi(p)}(m). \end{aligned} \tag{15}$$

The second equation is obtained by exploiting the convolution-preservation property of the DFnT that the Fresnel transform of a convolution of two signals equals the Fresnel transform of either one convolved with the other.

Inspecting (15), the received pilot on the p-th RX antenna is the superposition of the CIR from all the TX antennas to the p-th RX antenna shifted by $\{D_q\}$. In the above equations, as well as following discussion, considering the cyclic convolution, the domain of the sequences and functions, $\hat{h}_{p,q}(n)$, $y_{\Psi(p)}(n)$, and $h_{p,q}(n)$, etc., is a cyclic group of order N. That is, when imposing the sequence domain n with shift operation, one has

$$(n + D_q) \equiv (n + D_q) \mod N.$$

Considering the fact that the spread of real-world channels is time-limited, the CIR functions $h_{p,q}$ may still be recoverable if $\{D_q\}$ are carefully designed. Given that the maximum delay spread of the channel is L_{CIR}, which is in practice smaller than the length of CP, i.e., $L_{\mathrm{CIR}} < L_{\mathrm{CP}}$, one can easily prove that for any D_{q_1}, D_{q_2}, where $1 \le q_1, q_2 \le M_{\mathrm{T}}$ and $q_1 \ne q_2$, if

$$|D_{q_1} - D_{q_2}| > L_{\mathrm{CIR}}, \tag{16}$$

the CIR functions can be recovered without any inter-antenna interference. With the condition in (16), the CIR function from the q-th TX antenna to the p-th RX antenna can be estimated using merely shift operations, as

$$\begin{aligned} \hat{h}_{p,q}(n) &= \sqrt{\frac{1}{N}\frac{M_{\mathrm{T}}}{E_s}} y_{\Psi(p)}(n + D_q) \\ &= h_{p,q}(n) + \sqrt{\frac{1}{N}\frac{M_{\mathrm{T}}}{E_s}} w_{\Psi(p)}(n + D_q), \end{aligned} \tag{17}$$

by properly confining n. For simplicity, we consider that $\{D_q\}$ are in order, i.e., $0 \le D_1 < \cdots < D_{M_{\mathrm{T}}} \le N$, without loss of generality. Even if $\{D_q\}$ are not in order, we can always find a mapping $f_{\mathcal{Q}} : q \mapsto q'$, so that $\{D_{q'}\}$ are in order. Thereby, the estimated CIR functions are

$$\left\{ \hat{h}_{p,q}(n) \middle| n \in \mathcal{D}_q \right\}, \tag{18}$$

where $\mathcal{D}_q$ is the domain of $\hat{h}_{p,q}$ defined as

$$\mathcal{D}_q = \begin{cases} [0, D_{q+1} - D_q - 1] & \text{for } 1 \le q \le M_{\mathrm{T}} - 1 \\ [0, D_1 + N - 1 - D_q] & \text{for } q = M_{\mathrm{T}}. \end{cases} \tag{19}$$

The $M_R \times M_T$ CIR matrices can be formulated based on (18) to characterize the MIMO channel for signal recovery.

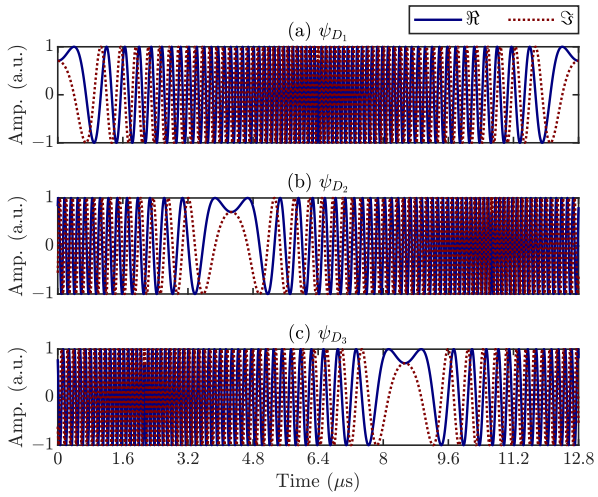

Fig. 2. Illustration of a set of chirped pilots for the (a) 1st, (b) 2nd, and (c) 3rd TX antennas in a MIMO-OCDM systems with $M_{\mathrm{T}} = 3$ TX antennas.

Briefly, in the proposed algorithm we carefully choose M_T orthogonal chirped pilots from the DFnT matrix, $\psi_{D_q}(n)$ as indicated in (14). At the receiver, the signal at each RX antenna after pulse compression is the superposition of the cyclically shifted CIR functions from different TX antennas, and these CIR functions are distinguishable. Regarding the choice of the chirped pilots, as long as the spacing of two pilots is larger than the maximum delay spread of the channel, referring to (16), there should be no inter-antenna interference at the receiver. The most intuitive way is to choose the chirped pilots uniformly with indices

$$D_q = \left\lfloor (q-1) \cdot \frac{N}{M_{\mathrm{T}}} \right\rfloor. \tag{20}$$

In this case, the domain of the (p, q)-th estimated CIR function, $\hat{h}_{p,q}$, can be simplified as

$$\mathcal{D}_q = \left[0, \left\lfloor \frac{N}{M_{\mathrm{T}}} \right\rfloor\right].$$

To show how the proposed algorithm works, we consider a 4×3 MIMO system with $N = 256$ for example. Firstly, three chirps are uniformly chosen from $\mathcal{A}_{\Psi}$ to be the pilots for transmission, as illustrated in Fig. 2, with $\{\vec{\psi}_{D_q} | D_q = 0, 85, 170 \text{ for } q = 0, 1, 2\}$. The chirped pilots are the cyclic shift of one another. After MIMO transmission, the received pilot signals will be the superposition of the transmitted pilots as indicated in (2). Pulse compression is achieved by performing a DFnT on the received pilot, given in (15). Fig. 3a provides a one-shot observation of the received pilot signals. It can be seen that the received pilots after pulse compression are the sum of the CIR functions from the different TX antennas with no interference between TX antennas. As a result, the CIR functions can be readily retrieved based on (17) for signal recovery and channel equalization. Finally, the CFR functions can be obtained by performing a fast Fourier transform (FFT) on (17) for single-tap frequency-domain equalization.

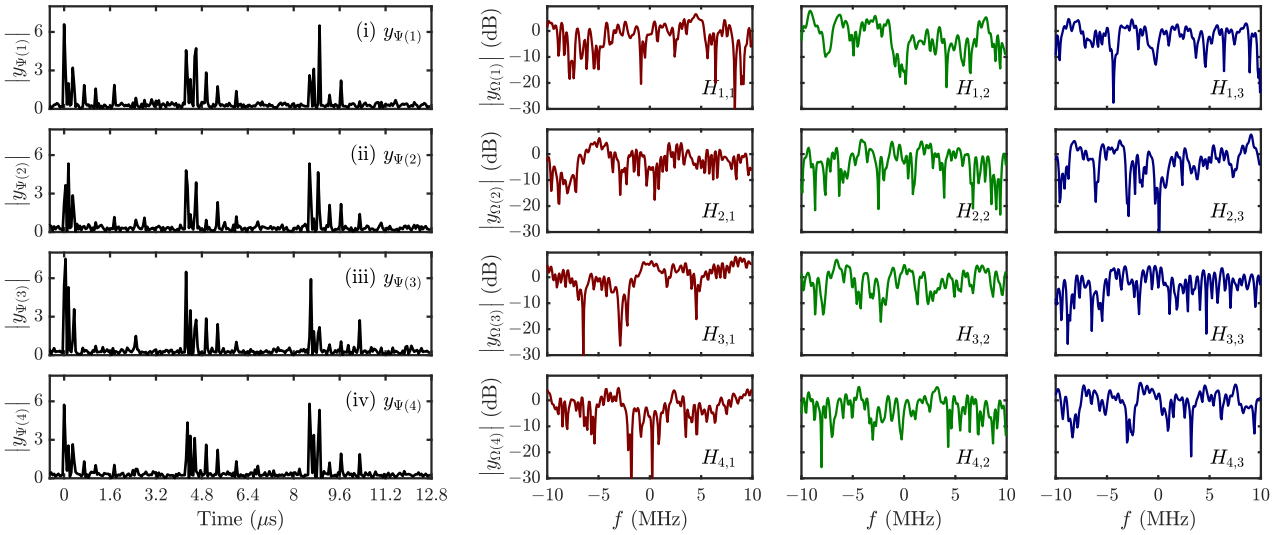

(a) Received overlapping CIRs after DFnT

(b) Recovered CFRs

Fig. 3. One-shot observation of a MIMO-OCDM system with 4 RX antennas and 3 TX antennas. (a) The received chirped pilots after DFnT at different Rx antennas; (b) The recovered channel frequency responses of the MIMO channel.

When FDE is adopted, the CFR functions can be obtained by FFTs, as

$$\begin{aligned}\hat{H}_{p,q}(m) &= \sqrt{N}\mathcal{F}_{\Omega}\left\{\hat{h}_{p,q}(n)\right\}(m)\\ &= H_{p,q}(m) + \sqrt{\frac{M_{\mathrm{T}}}{E_s}}\cdot w_{\Omega'(p,q)}(m),\end{aligned} \tag{21}$$

where $w_{\Omega'(p)}(m)$ is the frequency-domain noise defined as

$$w_{\Omega'(p,q)}(m) = \mathcal{F}_{\Omega}\left\{w_{\Psi(p)}(n+D_q)\right\}(m), \tag{22}$$

for $n \in \mathcal{D}_p$. Thus, the transfer matrix on the m-th frequency bin $\hat{\mathbf{\Lambda}}(m)$ is formed with its (p,q)-th element to be $\hat{H}_{p,q}(m)$ in (21). In Fig. 3b, the CFR functions of the MIMO system are recovered for illustration.

Although we showed the proposed algorithm for MIMO-OCDM systems above, it can be easily generalized for other types of MIMO-based systems, e.g., MIMO-OFDM systems. Since both OFDM and OCDM signals adopt cyclic prefix as the guard interval, OCDM signals are compatible with OFDM signals, and as a result, the OCDM-based pilots can be directly applied to traditional MIMO-OFDM systems, as well as other MIMO-based systems for channel estimation.

IV. Analysis and Discussions

In this section, we provide the performance analysis of the proposed channel estimation algorithm in comparison with the least-square (LS) channel estimator for the traditional MIMO-OFDM system. Discussion about the practical implementation for MIMO-OCDM systems is also provided, and an effective noise suppression algorithm introduced. We assume that the MIMO channel is linear and quasi-static, and stochastic. The additive noises are independent and identically distributed circularly symmetric Gaussian with zero means and variance N_0.

A. MSE Performance of the LS Estimator

Here, we will briefly analyze the MSE performance of the LS channel estimator for the MIMO-OFDM system [29], [54], [55]. In the LS estimator, in order to estimate the $M_{\mathrm{R}} \times M_{\mathrm{T}}$ transfer matrices, the ranks of the pilot matrices should be no less than that of the MIMO system. The pilot symbols should span over $M_{\mathrm{LS}}\,(\geq M_{\mathrm{T}})$ OFDM symbols with the assumption that the coherence time is much larger than $M_{\mathrm{LS}} \times T$. We formulate the pilot matrix on the m-th subcarrier as $\mathbf{X}_{\mathrm{LS}}(m) \in \mathbb{C}^{M_{\mathrm{T}}\times M_{\mathrm{LS}}}$ with its (q,l)-element to be the pilot on the q-th TX antenna and the l-th $(1 \leq l \leq M_{\mathrm{LS}})$ OFDM symbol. The pilot matrices have a power constraint that

$$\mathrm{Tr}\mathbf{X}_{\mathrm{LS}}(m)\,\mathbf{X}_{\mathrm{LS}}^{H}(m) = M_{\mathrm{T}}M_{\mathrm{LS}}, \tag{23}$$

where Tr$\cdot$ is the trace of a matrix. The power constraint is to make sure that the power of pilot signals is normalized with respect to the number of TX antennas [28]

The received pilot signal is

$$\mathbf{Y}_{\mathrm{LS}}(m) = \sqrt{\frac{E_s}{M_{\mathrm{T}}}}\mathbf{\Lambda}(m)\,\mathbf{X}_{\mathrm{LS}}(m) + \mathbf{W}_{\Omega}(m), \tag{24}$$

where $\mathbf{Y}_{\mathrm{LS}}(m) \in \mathbb{C}^{M_{\mathrm{R}}\times M_{\mathrm{LS}}}$ is the received pilot matrix on the m-th subcarrier with its (p,l)-th element to be the received pilot symbol on the p-th RX antenna and the l-th OFDM symbol, and $\mathbf{W}_{\Omega}(m) = [\mathbf{w}_1(m),\ldots,\mathbf{w}_{M_{\mathrm{LS}}}(m)] \in \mathbb{C}^{M_{\mathrm{R}}\times M_{\mathrm{LS}}}$ is the noise matrix in the frequency domain, such that

$$\mathcal{E}\left\{\mathbf{w}_{l_1}(m)\cdot\mathbf{w}_{l_2}^{H}(m)\right\} = N_0\delta(l_1-l_2)\cdot\mathbf{I}_{M_{\mathrm{R}}}.$$

The pilots are known at the receiver, and the LS estimation of the MIMO system can be obtained by

$$\hat{\mathbf{\Lambda}}_{\mathrm{LS}}(m) = \sqrt{\frac{M_{\mathrm{T}}}{E_s}}\mathbf{Y}_{\mathrm{LS}}(m)\cdot\mathbf{X}_{\mathrm{LS}}^{\dagger}(m), \tag{25}$$

and the MSE of the LS estimation is accordingly

$$\begin{aligned}\left|\epsilon_{\hat{\Lambda}_{\mathrm{LS}}}\right|^2 &= \mathcal{E}\left\{\frac{1}{N}\sum_{m=0}^{N-1}\left\|\hat{\mathbf{\Lambda}}_{\mathrm{LS}}(m)-\mathbf{\Lambda}(m)\right\|_F^2\right\}\\ &= \frac{1}{N}\mathcal{E}\left\{\sum_{m=0}^{N-1}\left\|\sqrt{\frac{M_{\mathrm{T}}}{E_s}}\mathbf{W}_{\Omega}(m)\,\mathbf{X}_{\mathrm{LS}}^{\dagger}(m)\right\|_F^2\right\}\end{aligned}$$

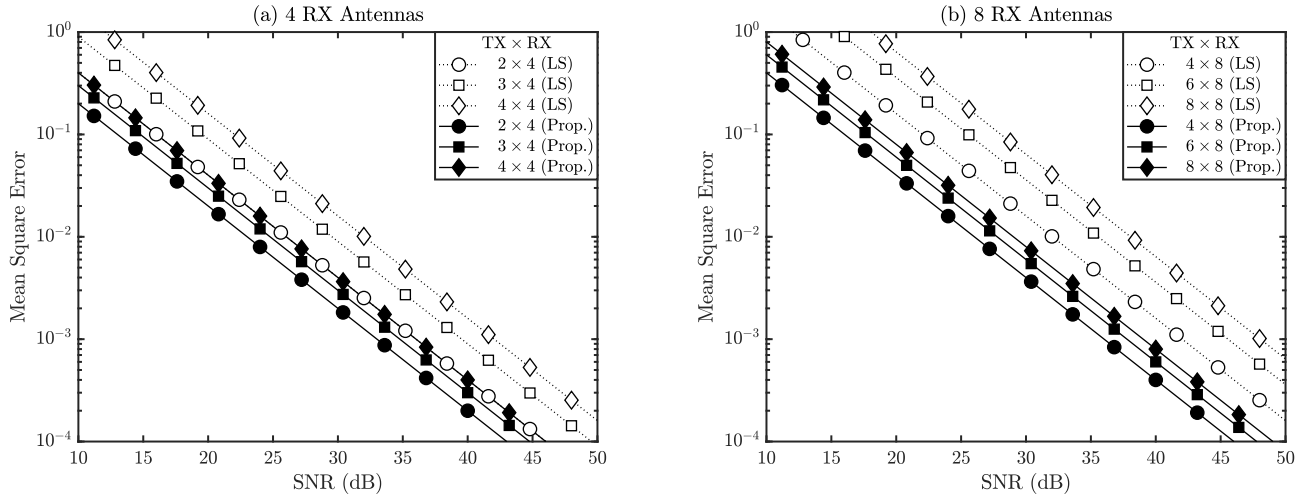

Fig. 4. Theoretical MSE performance of the proposed and LS estimators against SNR. Both estimators have the same overhead.

$$\geqslant \frac{M_{\mathrm{T}}^2 M_{\mathrm{R}}}{M_{\mathrm{LS}}} \cdot \rho^{-1}. \tag{26}$$

In the last equation, the equal sign holds if and only if (i.i.f) $\mathbf{X}_{\mathrm{LS}}$ are row-orthogonal matrices.

B. Performance Analysis of the Proposed Estimator

In this subsection, we first consider the case that the chirped pilots are transmitted using one OCDM symbol. Based on (21), the MSE of the proposed estimation is given by

$$\begin{aligned}\left|\epsilon_{\hat{\Lambda}_\Psi}\right|^2 &= \mathcal{E}\left\{\frac{1}{N}\sum_{m=0}^{N-1}\left\|\hat{\mathbf{\Lambda}}(m)-\mathbf{\Lambda}(m)\right\|_F^2\right\} \\ &= \frac{1}{N}\frac{M_{\mathrm{T}}}{E_s}\sum_{m=0}^{N-1}\mathcal{E}\left\{\left\|\mathbf{W}_{\Omega'}(m)\right\|_F^2\right\} \\ &= M_{\mathrm{T}}M_{\mathrm{R}}\cdot\frac{1}{\rho},\end{aligned} \tag{27}$$

where $\mathbf{W}_{\Omega'}(m) \in \mathbb{C}^{M_{\mathrm{R}}\times M_{\mathrm{T}}}$ is the noise matrix with its (p,q)-th element $w_{\Omega'(p,q)}(m)$ as defined in (22). The detailed derivation is provided in Appendix A. Moreover, the chirped pilots can be transmitted over multiple symbols to improve the estimation accuracy. For a fair comparison, we assume the same overhead as the LS estimator in Section IV-A, i.e., using M_{LS} symbols. The performance of the proposed estimator can be further improved by a factor of M_{LS}, as

$$\left|\epsilon_{\hat{\Lambda}_\Psi}\right|^2 = \frac{M_{\mathrm{T}}M_{\mathrm{R}}}{M_{\mathrm{LS}}}\cdot\rho^{-1}. \tag{28}$$

Comparing (26) and (28), we can see that the MSE of the proposed estimator is

$$\beta \equiv \frac{\left|\epsilon_{\hat{H}_\Psi}\right|^2}{\left|\epsilon_{\hat{H}_{\mathrm{LS}}}\right|^2} = \frac{1}{M_{\mathrm{T}}} \tag{29}$$

times that of the LS estimator. That is, with the same overhead, the performance of the proposed estimator is improved by a factor of M_{TX} when compared to the LS estimator.

In Fig. 4, the MSE performance of both the proposed and LS channel estimators are provided versus the received SNR considering different MIMO setups. In Fig. 4a, there are 4 RX antennas with different numbers of TX antennas; in Fig. 4b the number of RX antennas is 8. In both figures, the MSE of both estimators is proportional to the noise power. However, in terms of the number of TX antennas, M_{T}, the MSE of the proposed estimator is linearly proportional to M_{T}, while that of the LS estimator is proportional to M_{T}^2, as indicated in (26) and (28), respectively. In other words, the proposed estimator degrades slower than LS estimator as the number of TX antennas increases. In addition, comparing Fig. 4a and 4b, we can see that the performance improvement of the proposed algorithm increases with a larger number of TX/RX antennas. For example, for the 4×4 MIMO systems in Fig. 4a the proposed algorithm has about 6.5 dB SNR improvement over the LS algorithm to achieve a MSE of 10^{-3}, whilst for 8×8 MIMO in Fig. 4b, the SNR improvement increases to 9 dB at a MSE of 10^{-3}.

C. Discussions on Practical Implementation

To further improve the estimation accuracy in practical systems, smoothing/averaging algorithms will usually be applied to suppress the noise. For example, sliding average window (SAW) is an effective algorithm to improve the estimation accuracy adopted in the 4G/5G systems [56]. Once the CFRs are estimated through the pilots, as shown in (25), adjacent pilots are averaged in the frequency domain to suppress the noise,

$$\hat{H}_{\mathcal{S}(p,q)}(m) = \frac{1}{L_{\mathcal{S}}}\sum_{\eta\in\mathcal{S}}\hat{H}_{p,q}(m+\eta), \tag{30}$$

where $\mathcal{S}$ is the averaging window, defined as

$$\mathcal{S} = \left\{-\frac{L_{\mathcal{S}}-1}{2},\ldots,\frac{L_{\mathcal{S}}-1}{2}\right\},$$

and $L_{\mathcal{S}} \in \mathbb{N}\backslash 2\mathbb{N}$ is a positive odd number, denoting the width of the sliding window. Although the SAW algorithm is able to effectively suppress the noise by a factor of $L_{\mathcal{S}}$, it will distort the estimation, leading to a deviation from the actual channel under estimation. Especially, the wider the averaging window $L_{\mathcal{S}}$ is, the larger the deviation.

To elaborate this effect, the MSE of the LS estimation after SAW is given below, as

$$\begin{aligned}\left|\epsilon_{\Lambda_{\mathcal{S}}}\right|^2 &= \frac{1}{N}\mathcal{E}\left\{\sum_{m=0}^{N-1}\left\|\bar{\mathbf{\Lambda}}_{\mathcal{S}}(m)-\mathbf{\Lambda}(m)\right\|_F^2\right\}\\ &= M_{\mathrm{T}}M_{\mathrm{R}}\sum_{n=0}^{N-1}\left|\mathrm{sind}\left(\frac{\pi}{N}L_{\mathcal{S}}\cdot n\right)-1\right|^2\cdot\sigma_h^2(n)\\ &\quad+\frac{1}{L_{\mathcal{S}}}\frac{M_{\mathrm{T}}^2M_{\mathrm{R}}}{M_{\mathrm{LS}}}\rho^{-1},\end{aligned}\tag{31}$$

where $\sigma_h^2(n)$ is the power delay profile (PDP) of the channel, and $\sum\sigma_h^2(n)=1$. Please see Appendix B for more details. It can be seen that the MSE of the SAW estimation consists of two parts. The second term is the noise after average and is scaled by a factor of $1/L_{\mathcal{S}}$. The larger the $L_{\mathcal{S}}$ is, the smaller the noise is. On the other hand, the first term is about the PDP function, denoting the distortion of channel weighted by a Dirichlet sinc function. The width of the Dirichlet sinc function is inversely proportional to $L_{\mathcal{S}}$. The larger the $L_{\mathcal{S}}$ is, the worse the distortion becomes. Hence, the window width should be carefully designed. In the 4G/5G systems, $L_{\mathcal{S}}$ is in practice no greater than 19 as a balance between the noise suppression and the estimation deviation.

In the following, a more efficient and unbiased smoothing algorithm dedicated to the proposed estimator is introduced by exploiting the pulse-compression property of chirped waveforms. In the proposed algorithm, the received pilot signal after pulse compression, as shown in (15), is equivalent to the sum of the pilots from different TX antennas. Not only the pilots from unwanted TX antennas but also the noise exceeding the length of CIR can be removed. Utilizing the finite impulse response (FIR) of the channel, a more accurate estimation can be obtained by filtering out the excessive noise. To achieve this, we define a window function $\Pi_G(n)$. The function can be a rectangular function of width $L_{\mathcal{G}}$. Other types of window function can also be adopted to remove the excessive noise, such as the raised cosine function. The windowed CIR functions are accordingly obtained as

$$\hat{h}_{\mathcal{G}(p,q)}(n)=\Pi(n)\cdot\hat{h}_{p,q}(n).\tag{32}$$

If we take the rectangular function as the window for example, i.e., $\Pi_G(n)=1$ for $n=0,1,\ldots,L_{\mathcal{G}}-1$, and 0 otherwise, the MSE of the proposed algorithm is

$$\begin{aligned}\left|\epsilon_{\Lambda_{\mathcal{G}}}\right|^2 &= \mathcal{E}\left\{\left\|\mathbf{\Lambda}_{\mathcal{G}}(m)-\mathbf{\Lambda}(m)\right\|_F^2\right\}\\ &= M_{\mathrm{T}}M_{\mathrm{R}}\cdot\sum_{n=L_{\mathcal{G}}}^{N-1}\left|\sigma_h^2(n)\right|^2+\frac{L_{\mathcal{G}}}{N}\frac{M_{\mathrm{T}}^2M_{\mathrm{R}}}{M_{\mathrm{LS}}}\rho^{-1}.\end{aligned}\tag{33}$$

The detailed derivation is provided in Appendix C.

Comparing (31) and (33), the MSE of both estimators consists of two sub-terms; one is the PDP term and the other one is the noise term. However, in the proposed algorithm, the noise term is instead proportional to $L_{\mathcal{G}}$, and the smaller the window width $L_{\mathcal{G}}$ is, the smaller the noise becomes. This is because the proposed algorithm rejects the excessive noise beyond the window. Thus, we term it as noise-rejection window (NRW). In the NRW algorithm, the PDP term is the sum of the tail of the PDP function outside the window. Considering the FIR feature of real-world channels, that $|\sigma_h(n)|^2=0$ for $n\geq L_{\mathrm{CIR}}$, the estimation of the NRW is unbiased. The PDP term in (33) vanishes as long as the window is wider than the maximum delay spread of the channel.

It can be seen that although both algorithms can effectively suppress the noise effect, they behave differently. The SAW algorithm suppresses the noise by smoothing the CFR function, and the estimation deviates from the actual system as long as $L_{\mathcal{S}}$ is greater than 1. There is always a tradeoff between the noise and deviation yielding a sub-optimal performance. In the NRW algorithm, excessive noise is directly removed from the estimation after pulse compression. The estimation is unbiased if the window is wider than the maximum delay spread of the channel, i.e., $L_{\mathcal{G}}\geq L_{\mathrm{CIR}}$, and can optimally converge to the system under estimation. Even if the window width $L_{\mathcal{G}}$ is reasonably smaller than L_{CIR}, there will not be severe distortion because the tails of the CIR functions are usually much smaller than its main path. For example, for a channel with exponential PDP, which is applicable for most practical channels, the tail beyond 3 times of the root mean square (rms) delay spread is less than 5% of the total energy.

V. Simulations and Results

In this section, numerical results are provided to evaluate the performance of the propsoed channel estimation algorithm as analyzed in Section IV. The OCDM system has a bandwidth of 20 MHz with $N=2048$ chirps for modulation. The length of GI is 256. For a fair comparison, the OFDM system use the same bandwidth, which is divided into 2048 subcarriers, and the same GI length.

A. MSE Performance

To show the analytical results discussed in Section IV, we consider a multipath fading MIMO channel with an exponential PDP, which is a typical channel model in practical systems [57], [58], [59], [60]. The PDP function is defined as

$$\begin{aligned}\sigma_h^2(n) &= \mathcal{E}\left\{\left|h_{p,q}(nT_{\mathrm{s}})\right|^2\right\}\\ &= \frac{T_s}{\tau_0}e^{n\frac{T_s}{\tau_0}},\end{aligned}\tag{34}$$

where τ_0 is the rms delay spread of the channel and T_s is the sampling interval. Substituting (34) into (33), the analytical MSE can be further given by

$$\left|\epsilon_{\Lambda_{\mathcal{G}}}\right|^2=M_{\mathrm{T}}M_{\mathrm{R}}\cdot e^{-L_{\mathcal{G}}\frac{T_s}{\tau_0}}+\frac{L_{\mathcal{G}}}{N}\frac{M_{\mathrm{T}}^2M_{\mathrm{R}}}{M_{\mathrm{LS}}}\rho^{-1},\tag{35}$$

as derived in (45) in Appendix C. The optimal window width and the minimum MSE are given in (47) and (48), respectively.

In Fig. 5, the MSE of the proposed channel estimator with NRW algorithm is provided in contour diagrams as a function of the received SNR and the width of noise rejection window, with $\tau_0=$ (a) 0.4 μs and (b) 0.8 μs, respectively. Along the SNR axis, the MSE is a monotonic function, and it decreases along with the SNR axis. On the other hand, the MSE is a convex function with respect to the window width, $L_{\mathcal{G}}$. For a fixed SNR, there exists an optimal $L_{\mathcal{G}}$ yielding the minimum

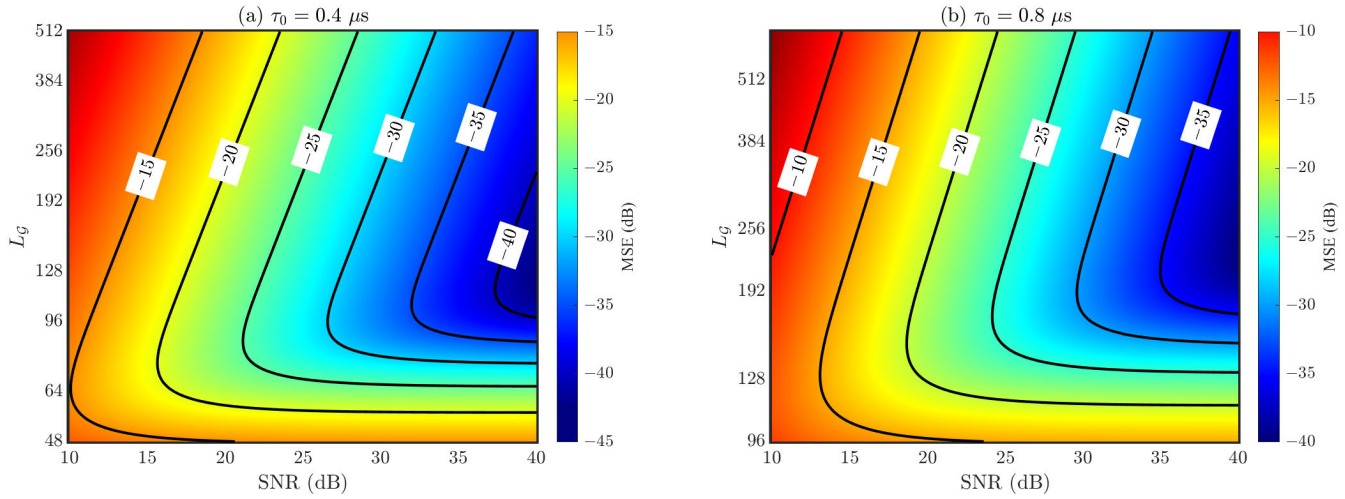

Fig. 5. MSE performance of the proposed estimator for a MIMO-OCDM system with 3 TX antennas and 4 RX antennas. The MSE is measured as a function of received SNR and window width in 2D contour plots. The PDPs of the channel have a rms delay of (a) $\tau_0 = 0.4$ μs and (b) $\tau_0 = 0.8$ μs, respectively.

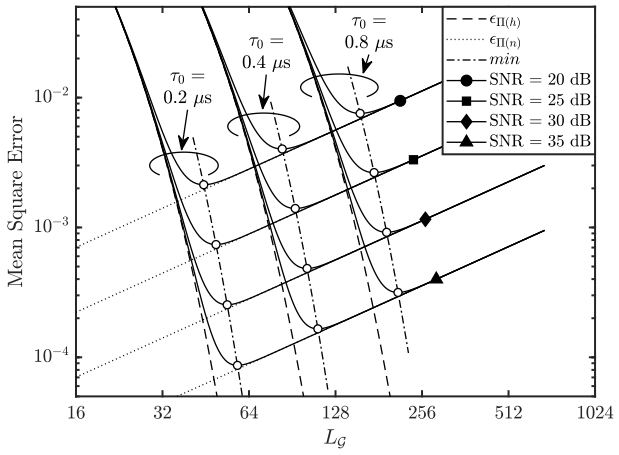

Fig. 6. Performance of the proposed estimator against the window width. The MSE performance (solid lines) are the sum of the noise term (dotted lines) and the distortion due to exceeding the window (dashed lines).

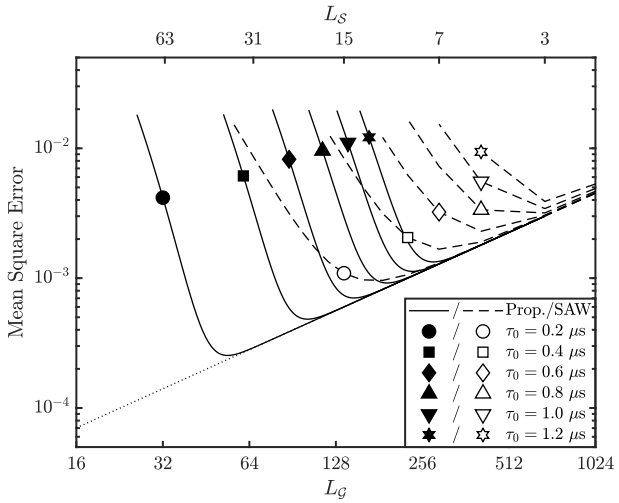

Fig. 7. Performance comparison of the proposed and SAW estimators with a received SNR = 30 dB. Both estimators are normalized to the same noise suppression capability as the noise terms (dotted lines) overlapped.

MSE. The optimal window width is given as a function of SNR (see (47) in Appendix C), as indicated by the dashed lines in Fig. 5. For a given SNR, a larger $L_\mathcal{G}$ allows more noise passing through but has much less deviation. When the window width is much larger than the delay spread of the system, $L_\mathcal{G} \gg \tau_0$, the remainder noise passing through the window determines the MSE performance. The MSE goes larger as $L_\mathcal{G}$ increases because the noise term is linearly proportional to the window width. When the window width is comparable to the delay spread, the MSE of the proposed estimator is the interplay of the noise and estimation deviation. However, when the widow width is relatively smaller than the delay spread, the deviation of the estimation will dominate the performance degradation. Especially, the MSE degrades dramatically as $L_\mathcal{G}$ decreases. Similar trend can be observed in Fig. 5a and 5b. The difference between them is that a larger delay spread results in worse performance, and the optimal window width is proportional to τ_0.

To show how the NRW algorithm behaves on performance, the CIR and noise terms are shown in Fig. 6, depicted with the dashed and the dotted lines, respectively. It can be seen that the noise term is inversely proportional to the window width, $L_\mathcal{G}$, as indicated in (35). For example, in the case of $\tau_0 = 0.4$ μs, the MSE curve is well fitted with the corresponding noise curve for $L_\mathcal{G} > 128$ ($16\tau_0$), and it increases with $L_\mathcal{G}$. The deviation of the CIR term in this case is less than -58 dB for $L_\mathcal{G} \geq 128$, which is negligible. As the window becomes narrower, the MSE begins to degrade dramatically, for $L_\mathcal{G} < 64$ ($8\tau_0$). In this case, the deviation is greater than -24 dB, and dominates the degradation on MSE. Similar trend can be observed in the cases of $\tau_0 = 0.2$ and 0.8 μs. The slope of the CIR curves are much steeper than that of the noise term as discussed in Fig. 5. This is because the deviation will increase exponentially as $L_\mathcal{G}$ becomes narrower. It also implies that an unbiased estimator is usually preferred in practice.

The MSEs of both the proposed and the SAW algorithms are compared in Fig. 7 to show their difference. It can be seen that both algorithms can effectively suppress the noise term as the dotted lines overlap for both algorithms. However, their MSE performances are quite different due to the deviation of the estimation. In the SAW algorithm, the averaging operation is performed in the frequency domain, and the CIR function is equivalent to being weighted by a Dirichlet sinc function.

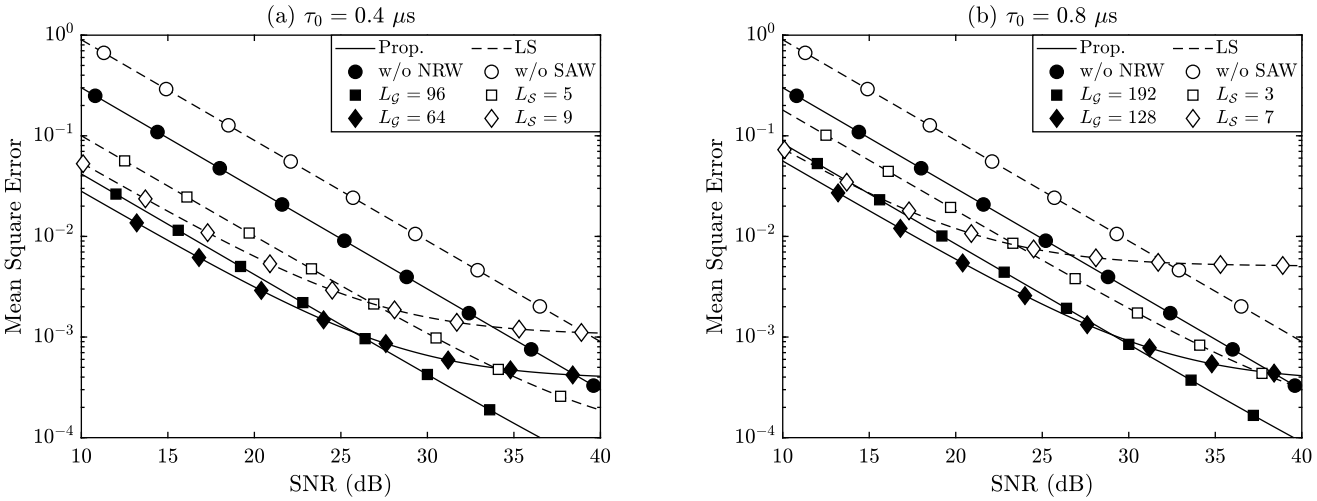

Fig. 8. MSE performance of the proposed estimator and the LS estimator with SAW algorithm as a function of received SNR with both systems equipped 3 TX antennas and 4 RX antenas. The MSE of both estimators without any smooth/average algorithms (circled lines) has no error floor, and the proposed estimator exhibits better sensitivity to the distortion than the SAW algorithm.

The SAW estimation always deviates from the MIMO system under estimation, i.e., $L_{\mathcal{S}} > 1$, as indicated by the dashed lines in Fig. 7[1]. In contrast, in the proposed estimator, there is "almost" no deviation until the window size is comparable to the delay spread of the channel. Strictly speaking, the proposed estimator is unbiased as long as $\sigma_h^2(n) = 0$ for $n > L_{\mathcal{G}}$.

Fig. 8 provides the MSE performance of both estimators as a function of SNR, for $\tau_0 = 0.4$ μs in Fig. 8a and $\tau_0 = 0.8$ μs in Fig. 8b, respectively. In Fig. 8a, the proposed algorithm requires 5 dB less SNR to achieve the same MSE than the LS estimator if there are no smoothing algorithms applied. For the proposed estimator, the MSE performance is improved when the NRW algorithm is applied. In Fig. 8a, the MSE reduces as the noise-rejection window width becomes smaller in the low SNR region. However, in the high SNR region, although there is no obvious degradation for $L_{\mathcal{G}} = 96$, the error floor occurs for $L_{\mathcal{G}} \leq 64$. This is because in the low SNR region, noise dominates the performance and the smaller the window width is, the less the noise effect is. As the SNR increases, the noise reduces, and the distortion due to the deviation after NRW begins to dominate for a small window width, e.g., $L_{\mathcal{G}} = 64$ for $\tau_0 = 0.4$ μs. For the LS estimator with SAW algorithm, as the averaging window increases, the MSE of the estimation decreases, especially in the low SNR region. However, error floors occur as long as SAW is applied. For example, in the case of $L_{\mathcal{S}} = 5$, slight degradation can be observed for SNR $>$ 35dB. In the case of $L_{\mathcal{S}} = 9$, obvious degradation can be observed for SNR $>$ 25dB, and an error floor at MSE $= 1 \times 10^{-3}$ exists. In contrast, even if the NRW algorithm has an error floor for a small $L_{\mathcal{G}}$, the error floor is much lower than for the SAW algorithm.

In Fig. 8b, similar trends can be observed, but the overall performance is worse as a result of larger delay spread. The error floor of the LS estimator becomes much more obvious for a larger τ_0. For example, the proposed algorithm with $L_{\mathcal{G}} = 192$ has no degradation, and the performance improves linearly along with the SNR. On the other hand, a slight degradation can be observed in the SAW algorithm even for a small $L_{\mathcal{S}} = 3$. As $L_{\mathcal{S}}$ increases to 7, although the performance outperforms the proposed estimator with $L_{\mathcal{G}} = 192$ for SNR < 15 dB, the performance degrades with an error floor at MSE $= 5 \times 10^3$. In particular, the error floor occurs in the proposed estimator only for $L_{\mathcal{G}} = 128$ with a BER $= 3 \times 10^{-4}$.

[1]In fact, if there is no delay spread, namely in the condition of $h_{p,q}(n) = \delta(n)$, SAW is also unbiased. However, this condition can be hardly satisfied in real wireless systems.

B. BER Performance

To evaluate the transmission performance of the proposed algorithm, in this subsection we implemented simulations on the bit error rate (BER) performance. In contrast to the previous subsection, we adopt a more practical 3GPP EVA channel model of a rms delay spread of 0.357 μs and a maximum delay spread of 2.51 μs, whose power delay profile can be found in [61]. Both the proposed algorithm and SAW algorithm are considered for the MIMO-OCDM system in Fig. 9. A 3×4 and a 6×8 MIMO-OCDM systems are respectively considered in Fig. 9a and 9b. In Fig. 9a, we can see that the proposed channel estimation algorithm has a BER floor at 7×10^{-4} with the noise rejection window $L_{\mathcal{G}} = 48$, which is equivalent to 2.4 μs, smaller than the maximum delay of the channel. In this case, although the noise is well rejected, the estimated CFR matrices are distorted compared to the actual channel. As long as $L_{\mathcal{G}} \geq 64$ (≥ 3.2 μs), is greater than the maximum delay spread, the BER performance of the MIMO-OCDM system approaches the BER performance of ideal channel estimation (dotted line). There is only about 1-dB SNR degradation when $L_{\mathcal{G}}$ increases from 64 to 512. On the other hand, when the SAW algorithm is applied, the performance improves as the averaging window increases from $L_{\mathcal{S}} = 1$, and is optimal for $L_{\mathcal{S}} = 11$ since the larger the averaging window, the smaller the noise power. However, the BER performance starts to degrade when $L_{\mathcal{S}} > 11$. There are error floors at 8×10^{-4} and 2×10^{-2} for $L_{\mathcal{S}} = 21$ and $L_{\mathcal{S}} = 43$, respectively. If $L_{\mathcal{S}} > 11$, the estimation deviation due to frequency-domain averaging becomes the dominant effect limiting the performance. We can infer that the actual BER performance is more sensitive to the estimation distortion

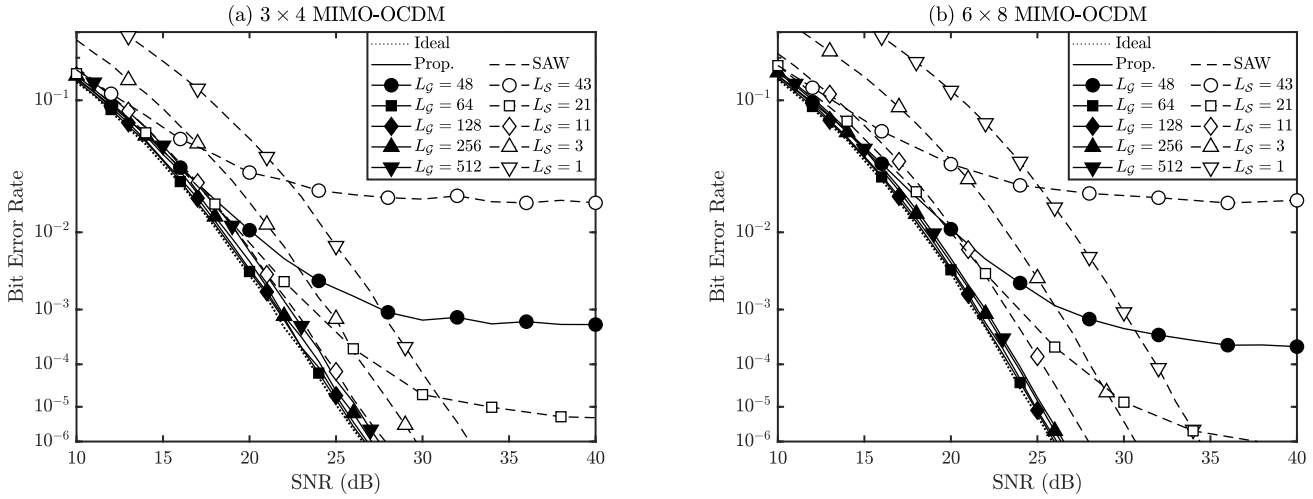

Fig. 9. BER performance of the MIMO-OCDM systems based on the proposed channel estimation algorithm with (a) 3×4 and 6×8 antennas.

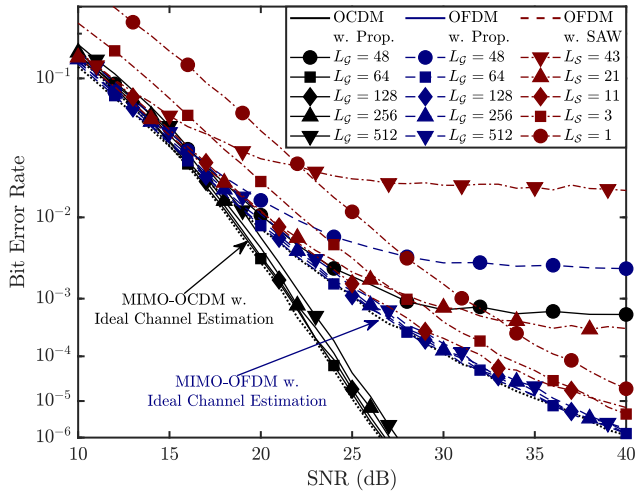

Fig. 10. BER performance of MIMO-OCDM and MIMO-OFDM systems based on the proposed channel estimation algorithm with 3×4 antennas.

or deviation from the actual channel than noise. In Fig. 9b, the BER performance of both algorithms behaves similarly to Fig. 9a.

To compare the performance between MIMO-OCDM and MIMO-OFDM systems, we apply the proposed algorithm and SAW algorithm for MIMO-OFDM systems. The former is compatible with MIMO-OFDM systems because the OCDM signal is compatible with OFDM systems, while the SAW algorithm is a standard channel estimation algorithm in actual 3GPP 4G/5G systems. The BER performance is evaluated in Fig. 10. The SAW algorithm has a similar performance trend in MIMO-OFDM; it improves the performance as $L_{\mathcal{S}}$ increase from 1 and is optimal at $L_{\mathcal{S}} = 11$, and then the BER performance starts to degrade as $L_{\mathcal{S}}$ increases. Nevertheless, the proposed channel estimation algorithm improves the performance of MIMO-OFDM signals when $L_{\mathcal{G}} \geq 64$ and outperforms the SAW algorithm. Even if $L_{\mathcal{S}} = 11$, the proposed algorithm has about 2 dB SNR improvement at a BER $= 1 \times 10^{-5}$. Moreover, the MIMO-OCDM system always outperforms the MIMO-OFDM system because OCDM signals are more robust to the multipath fading effect, as indicated in [7].

VI. Conclusion and Outlook

In this paper, a novel channel estimation algorithm adopting OCDM signals as pilots was proposed for emerging MIMO-OCDM systems. The algorithm exploits the pulse-compression and convolution-preservation properties of OCDM signals to improve estimation accuracy with only simple operations, and avoids inter-antenna interference. We show that the proposed channel estimation algorithm is unbiased with optimal MSE performance and can be generalized for MIMO systems with an arbitrary number of TX/RX antennas and other types of MIMO systems, for example, MIMO-OFDM systems. The proposed algorithm can be attractive for massive MIMO systems, which require more accurate channel acquisition co-existing with noise and interference; the orthogonal chirped waveforms hold the potential to mitigate the pilot contamination problem, which will be investigated in our following work focusing on massive MIMO-based OCDM systems. As a result, the proposed channel estimation algorithm is attractive for MIMO-based CSI estimation and makes the MIMO-OCDM system a promising air interface for a wide range of broadband wireless systems, such as, 5G+/6G and Wi-Fi, with backward compatibility with MIMO-OFDM systems.

Appendix A
Proof of the MSE of the Proposed Estimator

From the third equation in (27), the noise term is

$$\mathcal{E}\left\{\left\|\mathbf{W}_{\Omega}(m)\right\|_F^2\right\} = \sum_{p=1}^{M_{\mathrm{R}}}\sum_{q=1}^{M_{\mathrm{T}}}\left|w'_{\Omega(p,q)}(m)\right|^2 \tag{36}$$

where

$$w'_{\Omega(p,q)}(m) = \mathcal{F}_{\Omega}\left\{w_p(n+D_q)\right\}(m) \tag{37}$$

for $n = 0, 1, \ldots, D_{q+1}$. Substituting (88) and (88) back into (27), the MSE can be given as

$$\left|\epsilon_{\hat{\Lambda}_{\Psi}}\right|^2 = \frac{1}{N}\frac{M_{\mathrm{T}}}{E_s}\sum_{p=1}^{M_{\mathrm{R}}}\sum_{q=1}^{M_{\mathrm{T}}}\sum_{m=0}^{N-1}\left|\mathcal{F}_{\Omega}\left\{w_p(n+D_q)\right\}(m)\right|^2$$

$$= \frac{1}{N}\frac{M_{\mathrm{T}}}{E_s}\sum_{p=1}^{M_{\mathrm{R}}}\sum_{q=1}^{M_{\mathrm{T}}}\sum_{n=0}^{D_{q+1}-1}\left|w_p\left(n+D_q\right)\right|^2$$
$$= \frac{1}{N}\frac{M_{\mathrm{T}}}{E_s}\sum_{p=1}^{M_{\mathrm{R}}}\sum_{n=0}^{N-1}\left|w_p\left(n+D_q\right)\right|^2$$
$$= M_{\mathrm{T}}M_{\mathrm{R}}\cdot\rho^{-1}. \tag{38}$$

We can still prove that the noise terms are independent over different transmit antennas.

Appendix B
MSE of the SAW Algorithm

The MSE of the SAW formulated in (31) can be expanded by the definition of the Frobenius norm, as

$$\left|\epsilon_{\bar{\Lambda}_{\mathcal{S}}}\right|^2 = \mathcal{E}\left\{\frac{1}{N}\sum_{m=1}^{N}\left\|\hat{\mathbf{\Lambda}}_{\mathcal{S}}\left(m\right)-\mathbf{\Lambda}\left(m\right)\right\|_F^2\right\}$$
$$= \mathcal{E}\left\{\frac{1}{N}\sum_{m=1}^{N}\sum_{\substack{p\in\mathcal{M}_{\mathrm{R}}\\ q\in\mathcal{M}_{\mathrm{T}}}}\left|\hat{H}_{\mathcal{S}(p,q)}\left(m\right)-H_{p,q}\left(m\right)\right|^2\right\}. \tag{39}$$

The term $\hat{H}_{\mathcal{S}(p,q)}\left(m\right)$ can be split into two terms, as

$$\hat{H}_{\mathcal{S}(p,q)}\left(m\right) = \bar{H}_{p,q}\left(m\right)+\bar{w}_{p,q}\left(m\right), \tag{40}$$

in which the first term can be manipulated as

$$\bar{H}_{p,q}\left(m\right) = \frac{1}{|\mathcal{S}|}\sum_{\eta\in\mathcal{S}}H_{p,q}\left(m+\eta\right)$$
$$= \frac{\sqrt{N}}{|\mathcal{S}|}\cdot\sum_{\eta\in\mathcal{S}}\mathcal{F}\left\{h_{p,q}\left(n\right)\right\}\left(m+\eta\right)$$
$$= \sqrt{N}\cdot\mathcal{F}\left\{\mathrm{sind}\left(\frac{\pi}{N}D_{\Pi}n\right)h_{p,q}\left(n\right)\right\}\left(m\right), \tag{41}$$

where

$$\mathrm{sind}\left(\frac{\pi}{N}D_{\Pi}n\right) = \frac{\sin\frac{\pi}{N}D_{\Pi}n}{D_{\Pi}\sin\frac{\pi}{N}n}$$

is the Dirichlet sinc function. The second term is

$$\bar{w}_{p,q}\left(m\right) = \frac{1}{|\mathcal{S}|}\sum_{\eta\in\mathcal{S}}w_{p,q}\left(m+\eta\right), \tag{42}$$

and one can be easily prove that

$$\bar{w}_{p,q}\left(m\right)\sim\mathcal{N}\left(0,\frac{N_0}{|\mathcal{S}|}\right).$$

Substituting (34) and (40)–(42) back into (39), the MSE of the SAW estimation can be given in (43), shown at the bottom of the page. It can be seen that, except to the noise term that is inversely scaled by $|\mathcal{S}|$, the first term on the right hand side of the third equation is the term representing the deviation of the estimation.

Appendix C
MSE of the Proposed Algorithm

The MSE of the proposed NRW algorithm in (33) can be expanded as

$$\left|\epsilon_{\Lambda_{\mathcal{G}}}\right|^2 = \sum_{\substack{p\in\mathcal{M}_{\mathrm{R}}\\ q\in\mathcal{M}_{\mathrm{T}}}}\mathcal{E}\left\{\frac{1}{N}\sum_{m=0}^{N-1}\left|\hat{H}_{\mathcal{G}(p,q)}\left(m\right)-H_{p,q}\left(m\right)\right|^2\right\}$$
$$= \sum_{\substack{p\in\mathcal{M}_{\mathrm{R}}\\ q\in\mathcal{M}_{\mathrm{T}}}}\mathcal{E}\left\{\sum_{m=0}^{N-1}\left|\hat{h}_{\mathcal{G}(p,q)}\left(m\right)-h_{p,q}\left(m\right)\right|^2\right\}$$
$$= \sum_{\substack{p\in\mathcal{M}_{\mathrm{R}}\\ q\in\mathcal{M}_{\mathrm{T}}}}\mathcal{E}\left\{\sum_{m=L_{\mathcal{G}}}^{N-1}\left|h_{p,q}\left(m\right)\right|^2+\frac{1}{N}\frac{M_{\mathrm{T}}}{E_s}\sum_{m=0}^{L_{\mathcal{G}}-1}\left|w_{\Psi}\right|^2\right\}. \tag{44}$$

Substitute (34) into (44), it becomes

$$\left|\epsilon_{\Lambda_{\mathcal{G}}}\right|^2 = M_{\mathrm{T}}M_{\mathrm{R}}\sum_{n=L_{\mathcal{G}}}^{N-1}\frac{1}{T_s}e^{-n\frac{T_s}{\tau_0}}+\frac{L_{\mathcal{G}}}{N}M_{\mathrm{T}}^2M_{\mathrm{R}}\rho^{-1}$$
$$= M_{\mathrm{T}}M_{\mathrm{R}}e^{-L_{\mathcal{G}}\frac{T_s}{\tau_0}}+\frac{L_{\mathcal{G}}}{N}M_{\mathrm{T}}^2M_{\mathrm{R}}\rho^{-1}. \tag{45}$$

In addition, we can derive the minimum MSE with respect to the gate size as

$$\frac{\partial\left|\epsilon_{\Lambda_{\mathcal{G}}}\right|^2}{\partial L_{\mathcal{G}}} = M_{\mathrm{T}}M_{\mathrm{R}}\frac{T_s}{\tau_0}e^{-L_{\mathcal{G}}\frac{T_s}{\tau_0}}+\frac{M_{\mathrm{T}}^2M_{\mathrm{R}}}{N}\rho^{-1} \tag{46}$$

to get the optimum window width

$$L_{\mathcal{G}} = \frac{\tau_0}{T_s}\ln\left(\rho\frac{T}{\tau_0}\frac{M_{\mathrm{LS}}}{M_{\mathrm{T}}}\right) \tag{47}$$

$$\left|\epsilon_{\bar{\Lambda}_{\mathcal{S}}}\right|^2 = \frac{1}{N}\sum_{\substack{p\in\mathcal{M}_{\mathrm{R}}\\ q\in\mathcal{M}_{\mathrm{T}}}}\left[\mathcal{E}\left\{\sum_{m=0}^{N-1}\left|\bar{H}_{p,q}\left(m\right)-H_{p,q}\left(m\right)\right|^2\right\}+\mathcal{E}\left\{\sum\left|\bar{w}_{p,q}\left(m\right)\right|^2\right\}\right]$$
$$= \frac{1}{N}\sum_{\substack{p\in\mathcal{M}_{\mathrm{R}}\\ q\in\mathcal{M}_{\mathrm{T}}}}\left[N\cdot\sum_{n=0}^{N-1}\left|\mathrm{sind}\left(\frac{\pi}{N}D_{\Pi}n\right)-1\right|^2\mathcal{E}\left\{\left|h_{p,q}\left(n\right)\right|^2\right\}+\frac{1}{|\mathcal{S}|}\sum_{m=0}^{N-1}\mathcal{E}\left\{\left|\bar{w}_{p,q}\left(m\right)\right|^2\right\}\right]$$
$$= M_{\mathrm{T}}M_{\mathrm{R}}\sum_{n=0}^{N-1}\left\{\left|\mathrm{sind}\left(\frac{\pi}{N}D_{\Pi}n\right)-1\right|^2\cdot\frac{T_s}{\tau_0}e^{-n\frac{T_s}{\tau_0}}\right\}+\frac{1}{|\mathcal{S}|}\frac{M_{\mathrm{T}}^2M_{\mathrm{R}}}{M_{\mathrm{LS}}}\rho^{-1}. \tag{43}$$

and the minimum MSE is obtained by substituting (47) back to (45)

$$|\epsilon_{\Lambda_\mathcal{G}}|^2 = \frac{M_\mathrm{T}^2 M_\mathrm{R}}{M_\mathrm{LS}} \frac{\tau_0}{T} \rho^{-1} \left[1 + \ln \left(\frac{M_\mathrm{LS}}{M_\mathrm{T}} \frac{T}{\tau_0} \rho \right) \right], \tag{48}$$

where $T = N \cdot T_s$ is the length of an OCDM symbol.

REFERENCES

[1] P. Wang, Y. Li, L. Song, and B. Vucetic, "Multi-gigabit millimeter wave wireless communications for 5G: From fixed access to cellular networks," *IEEE Commun. Mag.*, vol. 53, no. 1, pp. 168–178, Jan. 2015.

[2] L. Lu, G. Y. Li, A. L. Swindlehurst, A. Ashikhmin, and R. Zhang, "An overview of massive MIMO: Benefits and challenges," *IEEE J. Sel. Topics Signal Process.*, vol. 8, no. 5, pp. 742–758, Oct. 2014.

[3] P. Banelli, S. Buzzi, G. Colavolpe, A. Modenini, F. Rusek, and A. Ugolini, "Modulation formats and waveforms for 5G networks: Who will be the heir of OFDM: An overview of alternative modulation schemes for improved spectral efficiency," *IEEE Signal Process. Mag.*, vol. 31, no. 6, pp. 80–93, Nov. 2014.

[4] S. D. Liyanaarachchi, T. Riihonen, C. B. Barneto, and M. Valkama, "Optimized waveforms for 5G–6G communication with sensing: Theory, simulations and experiments," *IEEE Trans. Wireless Commun.*, vol. 20, no. 12, pp. 8301–8315, Dec. 2021.

[5] Y. Kim et al., "New radio (NR) and its evolution toward 5G-advanced," *IEEE Wireless Commun.*, vol. 26, no. 3, pp. 2–7, Jun. 2019.

[6] M. A. Uusitalo et al., "Hexa-X the European 6G flagship project," in *Proc. Joint Eur. Conf. Netw. Commun. 6G Summit (EuCNC/6G Summit)*, Jun. 2021, pp. 580–585.

[7] X. Ouyang and J. Zhao, "Orthogonal chirp division multiplexing," *IEEE Trans. Commun.*, vol. 64, no. 9, pp. 3946–3957, Sep. 2016.

[8] X. Ouyang and J. Zhao, "Orthogonal chirp division multiplexing for coherent optical fiber communications," *J. Lightw. Technol.*, vol. 34, no. 18, pp. 4376–4386, Sep. 15, 2016.

[9] X. Ouyang, O. A. Dobre, Y. L. Guan, and J. Zhao, "Chirp spread spectrum toward the Nyquist signaling rate—Orthogonality condition and applications," *IEEE Signal Process. Lett.*, vol. 24, no. 10, pp. 1488–1492, Oct. 2017.

[10] X. Ouyang, G. Talli, M. Power, and P. Townsend, "Orthogonal chirp-division multiplexing for IM/DD-based short-reach systems," *Opt. Exp.*, vol. 27, no. 16, p. 23620–23632, Aug. 2019.

[11] Y. Bai and P.-J. Bouvet, "Orthogonal chirp division multiplexing for underwater acoustic communication," *Sensors*, vol. 18, no. 11, p. 3815, Nov. 2018. [Online]. Available: https://www.mdpi.com/1424-8220/18/11/3815

[12] L. Giroto de Oliveira, B. Nuss, M. B. Alabd, A. Diewald, M. Pauli, and T. Zwick, "Joint radar-communication systems: Modulation schemes and system design," *IEEE Trans. Microw. Theory Techn.*, vol. 70, no. 3, pp. 1521–1551, Mar. 2022.

[13] C. Browning, D. Dass, P. Townsend, and X. Ouyang, "Orthogonal chirp-division multiplexing for future converged optical/millimeter-wave radio access networks," *IEEE Access*, vol. 10, pp. 3571–3579, 2022.

[14] L. Cimini, "Analysis and simulation of a digital mobile channel using orthogonal frequency division multiplexing," *IEEE Trans. Commun.*, vol. COM-33, no. 7, pp. 665–675, Jul. 1985.

[15] J. Armstrong, "OFDM for optical communications," *J. Lightw. Technol.*, vol. 27, no. 3, pp. 189–204, Feb. 1, 2009.

[16] B. Farhang-Boroujeny and H. Moradi, "OFDM inspired waveforms for 5G," *IEEE Commun. Surveys Tuts.*, vol. 18, no. 4, pp. 2474–2492, 4th Quart., 2016.

[17] L. Yang and G. B. Giannakis, "Ultra-wideband communications—An idea whose time has come," *IEEE Signal Process. Mag.*, vol. 21, no. 6, pp. 26–54, Nov. 2004.

[18] H. Liu, "Multicode ultra-wideband scheme using chirp waveforms," *IEEE J. Sel. Areas Commun.*, vol. 24, no. 4, pp. 885–891, Apr. 2006.

[19] I. Dotlic and R. Kohno, "Low complexity chirp pulsed ultra-wideband system with near-optimum multipath performance," *IEEE Trans. Wireless Commun.*, vol. 10, no. 1, pp. 208–218, Jan. 2011.

[20] M. D. Larsen, A. L. Swindlehurst, and T. Svantesson, "Performance bounds for MIMO-OFDM channel estimation," *IEEE Trans. Signal Process.*, vol. 57, no. 5, pp. 1901–1916, May 2009.

[21] S. Schwarz and M. Rupp, "Society in motion: Challenges for LTE and beyond mobile communications," *IEEE Commun. Mag.*, vol. 54, no. 5, pp. 76–83, May 2016.

[22] H. Ji et al., "Overview of full-dimension MIMO in LTE-advanced pro," *IEEE Commun. Mag.*, vol. 55, no. 2, pp. 176–184, Feb. 2017.

[23] C. Shin, R. W. Heath Jr., and E. J. Powers, "Blind channel estimation for MIMO-OFDM systems," *IEEE Trans. Veh. Technol.*, vol. 56, no. 2, pp. 670–685, Mar. 2007.

[24] X. Ouyang, C. Antony, G. Talli, and P. D. Townsend, "Robust channel estimation for coherent optical orthogonal chirp-division multiplexing with pulse compression and noise rejection," *J. Lightw. Technol.*, vol. 36, no. 23, pp. 5600–5610, Dec. 2018.

[25] Y. G. Li, J. H. Winters, and N. R. Sollenberger, "MIMO-OFDM for wireless communications: Signal detection with enhanced channel estimation," *IEEE Trans. Commun.*, vol. 50, no. 9, pp. 1471–1477, Sep. 2002.

[26] J. Yue, K. Jin Kim, J. D. Gibson, and R. A. Iltis, "Channel estimation and data detection for MIMO-OFDM systems," in *Proc. IEEE Global Telecommun. Conf.*, Dec. 2003, pp. 581–585.

[27] I. Barhumi, G. Leus, and M. Moonen, "Optimal training design for MIMO OFDM systems in mobile wireless channels," *IEEE Trans. Signal Process.*, vol. 51, no. 6, pp. 1615–1624, Jun. 2003.

[28] H. Minn and N. Al-Dhahir, "Optimal training signals for MIMO OFDM channel estimation," *IEEE Trans. Wireless Commun.*, vol. 5, no. 5, pp. 1158–1168, May 2006.

[29] M. Biguesh and A. B. Gershman, "Training-based MIMO channel estimation: A study of estimator tradeoffs and optimal training signals," *IEEE Trans. Signal Process.*, vol. 54, no. 3, pp. 884–893, Mar. 2006.

[30] M. K. Ozdemir and H. Arslan, "Channel estimation for wireless OFDM systems," *IEEE Commun. Surveys Tuts.*, vol. 9, no. 2, pp. 18–48, 2nd Quart., 2007.

[31] Y. Liu, Z. Tan, H. Hu, L. J. Cimini, and G. Y. Li, "Channel estimation for OFDM," *IEEE Commun. Surveys Tuts.*, vol. 16, no. 4, pp. 1891–1908, 4th Quart., 2014.

[32] S. Hu, Z. Liu, Y. L. Guan, C. Jin, Y. Huang, and J. Wu, "Training sequence design for efficient channel estimation in MIMO-FBMC systems," *IEEE Access*, vol. 5, pp. 4747–4758, 2017.

[33] A. van Zelst and T. C. W. Schenk, "Implementation of a MIMO OFDM-based wireless LAN system," *IEEE Trans. Signal Process.*, vol. 52, no. 2, pp. 483–494, Feb. 2004.

[34] M. Šimko, Q. Wang, and M. Rupp, "Optimal pilot symbol power allocation under time-variant channels," *EURASIP J. Wireless Commun. Netw.*, vol. 2012, no. 1, p. 225, Jul. 2012.

[35] X. He, R. Song, and W.-P. Zhu, "Pilot allocation for sparse channel estimation in MIMO-OFDM systems," *IEEE Trans. Circuits Syst. II, Exp. Briefs*, vol. 60, no. 9, pp. 612–616, Sep. 2013.

[36] J. Ma et al., "Scattered pilot pattern and channel estimation method for MIMO-OFDM systems," U.S. Patent 14 520 080, Oct. 6, 2015.

[37] *5G; NR; Physical Channels and Modulation*, document TS 38.211, Version 17.3.0, 3rd Generation Partnership Project (3GPP), Sep. 2022.

[38] X. Lin et al., "5G new radio: Unveiling the essentials of the next generation wireless access technology," *IEEE Commun. Standards Mag.*, vol. 3, no. 3, pp. 30–37, Sep. 2019.

[39] S. Adireddy, L. Tong, and H. Viswanathan, "Optimal placement of training for frequency-selective block-fading channels," *IEEE Trans. Inf. Theory*, vol. 48, no. 8, pp. 2338–2353, Aug. 2002.

[40] Q. Huang, M. Ghogho, and S. Freear, "Pilot design for MIMO OFDM systems with virtual carriers," *IEEE Trans. Signal Process.*, vol. 57, no. 5, pp. 2024–2029, May 2009.

[41] A. Y. Panah, R. G. Vaughan, and R. W. Heath, "Optimizing pilot locations using feedback in OFDM systems," *IEEE Trans. Veh. Technol.*, vol. 58, no. 6, pp. 2803–2814, Jul. 2009.

[42] M. Simko, P. S. R. Diniz, Q. Wang, and M. Rupp, "Adaptive pilot-symbol patterns for MIMO OFDM systems," *IEEE Trans. Wireless Commun.*, vol. 12, no. 9, pp. 4705–4715, Sep. 2013.

[43] X. Ma, F. Yang, S. Liu, J. Song, and Z. Han, "Sparse channel estimation for MIMO-OFDM systems in high-mobility situations," *IEEE Trans. Veh. Technol.*, vol. 67, no. 7, pp. 6113–6124, Jul. 2018.

[44] M. B. Mashhadi and D. Gündüz, "Pruning the pilots: Deep learning-based pilot design and channel estimation for MIMO-OFDM systems," *IEEE Trans. Wireless Commun.*, vol. 20, no. 10, pp. 6315–6328, Oct. 2021.

[45] S. Joon Lee, "On the training of MIMO-OFDM channels with least square channel estimation and linear interpolation," *IEEE Commun. Lett.*, vol. 12, no. 2, pp. 100–102, Feb. 2008.

[46] V. Savaux and Y. Louët, "LMMSE channel estimation in OFDM context: A review," *IET Signal Process.*, vol. 11, no. 2, pp. 123–134, Apr. 2017.

[47] O. Edfors, M. Sandell, J.-J. van de Beek, S. K. Wilson, and P. O. Borjesson, "OFDM channel estimation by singular value decomposition," *IEEE Trans. Commun.*, vol. 46, no. 7, pp. 931–939, Jul. 1998.
[48] M. Diallo, R. Rabineau, and L. Cariou, "Robust DCT based channel estimation for MIMO-OFDM system," in *Proc. IEEE Wireless Commun. Netw. Conf.*, Apr. 2009, pp. 1–5.
[49] Z. Zhou, J. Fang, L. Yang, H. Li, Z. Chen, and R. S. Blum, "Low-rank tensor decomposition-aided channel estimation for millimeter wave MIMO-OFDM systems," *IEEE J. Sel. Areas Commun.*, vol. 35, no. 7, pp. 1524–1538, Jul. 2017.
[50] Tang, Zhou, and Wang, "Singular value decomposition channel estimation in STBC MIMO-OFDM system," *Appl. Sci.*, vol. 9, no. 15, p. 3067, Jul. 2019. [Online]. Available: https://www.mdpi.com/2076-3417/9/15/3067
[51] O. Elijah, C. Y. Leow, T. A. Rahman, S. Nunoo, and S. Z. Iliya, "A comprehensive survey of pilot contamination in massive MIMO—5G system," *IEEE Commun. Surveys Tuts.*, vol. 18, no. 2, pp. 905–923, 2nd Quart., 2016.
[52] X. Ouyang, C. Antony, F. Gunning, H. Zhang, and Y. L. Guan, "Discrete Fresnel transform and its circular convolution," 2015, *arXiv:1510.00574*.
[53] X. Ouyang, O. Dobre, Y. L. Guan, and P. Townsend, "Channel estimation for MIMO-OCDM systems as an emerging 6G radio access technology," in *Proc. IEEE Globecom Workshops (GC Wkshps)*, Dec. 2022, pp. 1573–1578.
[54] E. Karami, "Tracking performance of least squares MIMO channel estimation algorithm," *IEEE Trans. Commun.*, vol. 55, no. 11, pp. 2201–2209, Nov. 2007.
[55] P. Xu, J. Wang, J. Wang, and F. Qi, "Analysis and design of channel estimation in multicell multiuser MIMO OFDM systems," *IEEE Trans. Veh. Technol.*, vol. 64, no. 2, pp. 610–620, Feb. 2015.
[56] X. Dai, W. Zhang, J. Xu, J. E. Mitchell, and Y. Yang, "Kalman interpolation filter for channel estimation of LTE downlink in high-mobility environments," *EURASIP J. Wireless Commun. Netw.*, vol. 2012, no. 1, p. 232, Jul. 2012.
[57] V. Erceg et al., "A model for the multipath delay profile of fixed wireless channels," *IEEE J. Sel. Areas Commun.*, vol. 17, no. 3, pp. 399–410, Mar. 1999.
[58] Y. Wang, W.-J. Lu, and H.-B. Zhu, "Propagation characteristics of the LTE indoor radio channel with persons at 2.6 GHz," *IEEE Antennas Wireless Propag. Lett.*, vol. 12, pp. 991–994, 2013.
[59] D. W. Matolak, K. A. Remley, C. Holloway, and C. Gentile, "Outdoor-to-indoor channel dispersion and power-delay profile models for the 700-MHz and 4.9-GHz bands," *IEEE Antennas Wireless Propag. Lett.*, vol. 15, pp. 441–443, 2016.
[60] J. Ko et al., "Millimeter-wave channel measurements and analysis for statistical spatial channel model in in-building and urban environments at 28 GHz," *IEEE Trans. Wireless Commun.*, vol. 16, no. 9, pp. 5853–5868, Sep. 2017.
[61] *Evolved Universal Terrestrial Radio Access (E-UTRA); Relay Radio Transmission and Reception*, document TS36.116, 3GPP, 2018.

Xing Ouyang (Member, IEEE) received the Ph.D. degree from University College Cork, Cork, Ireland, in 2017. He is currently a Senior Researcher with the Tyndall National Institute, University College Cork. His research interests include high-speed fiber-optic and wireless communications, microwave photonics and radio-over-fiber systems, digital signal processing, and integrated sensing and communications. Moreover, he is recognized as the inventor of orthogonal chirp-division multiplexing (OCDM), which is an emerging multicarrier modulation technology for future high-speed optical and wireless access systems and radar systems, and based on the technology he is leading a research and development team for a pre-commercialization initiative, ChirpComm.

Octavia A. Dobre (Fellow, IEEE) received the Dipl.Ing. and Ph.D. degrees from the Polytechnic Institute of Bucharest, Romania, in 1991 and 2000, respectively.

From 2002 and 2005, she was with the New Jersey Institute of Technology, USA. In 2005, she joined the Memorial University of Newfoundland, Canada, where she is currently a Professor and the Canada Research Chair Tier 1. She was a Visiting Professor with the Massachusetts Institute of Technology, USA, and Université de Bretagne Occidentale, France. Her research interests include wireless communication and networking technologies, as well as optical and underwater communications. She has coauthored more than 450 refereed articles in these areas.

Dr. Dobre is elected as a member of the European Academy of Sciences and Arts and a fellow of the Engineering Institute of Canada and the Canadian Academy of Engineering. She was a recipient of the Best Paper Awards at various conferences, including IEEE ICC, IEEE Globecom, IEEE WCNC, and IEEE PIMRC. She serves as the Director of the Journals of the Communications Society. She was the inaugural Editor-in-Chief (EiC) of the IEEE OPEN JOURNAL OF THE COMMUNICATIONS SOCIETY and the EiC of the IEEE COMMUNICATIONS LETTERS. She served as the general chair, the technical program co-chair, the tutorial co-chair, and the technical co-chair of symposia at numerous conferences. She was a Fulbright Scholar, a Royal Society Scholar, and a Distinguished Lecturer of the IEEE Communications Society.

Yong Liang Guan (Senior Member, IEEE) received the B.E. degree (Hons.) from the National University of Singapore and the Ph.D. degree from Imperial College London, U.K. He is currently a Professor of communication engineering with the School of Electrical and Electronic Engineering, Nanyang Technological University (NTU), Singapore, where he leads the Continental-NTU Corporate Research Laboratory and the successful deployment of the campus-wide NTU-NXP V2X Test Bed. He has published an invited monograph, two books, and more than 450 journal and conference papers. He has secured more than U.S. $70 million of external research funding. He has 15 filed patents and three granted patents, one of which was licensed to NXP Semiconductors. His research interests include coding and signal processing for communication systems and data storage systems. He is an Editor of the IEEE TRANSACTIONS ON VEHICULAR TECHNOLOGY. He is also an Associate Vice President of NTU and a Distinguished Lecturer of the IEEE Vehicular Technology Society.

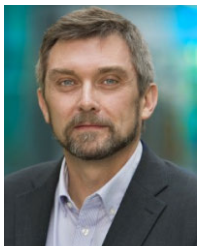

Paul Townsend (Senior Member, IEEE) received the Ph.D. degree in physics from the University of Cambridge, Cambridge, U.K., in 1987. From 1987 and 1990, he was a Research Fellow with the St John's College, Cambridge, and Bell Communications Research (Bellcore), Red Bank, NJ, USA, where he worked on non-linear optical switching phenomena in polymeric semiconductors. In 1990, he joined British Telecom (BT) Laboratories, U.K., as a Senior Staff Researcher to lead activities on Quantum Communications and Cryptography. In 2001, he joined the Corning Research Centre, U.K., as the Head of Group for Access Network Research. Since 2003, he has been with the Tyndall National Institute, University College Cork (UCC), Ireland, where he is currently the Head of Photonics Research, the Director of the Science Foundation Ireland, IPIC National Photonics Research Centre, and a Professor of photonic systems research with the School of Physics. He has coauthored more than 250 publications, including 35 invited conference papers, and holds granted patents in 16 families. His research interests include photonic systems and enabling technologies for optical communications. He is a fellow of the Institute of Physics (U.K. and Ireland).